Biomaterials 37 (2015) 469–477

Contents lists available at ScienceDirect

Biomaterials

journal homepage: www.elsevier.com/locate/biomaterials

Near-infrared labeled, ovalbumin loaded polymeric nanoparticles based on a hydrophilic polyester as model vaccine: *In vivo* tracking and evaluation of antigen-specific CD8$^+$ T cell immune response

Sima Rahimian [a, 1], Jan Willem Kleinovink [b, 1], Marieke F. Fransen [b], Laura Mezzanotte [c], Henrik Gold [d], Patrick Wisse [d], Hermen Overkleeft [d], Maryam Amidi [a], Wim Jiskoot [e], Clemens W. Löwik [c], Ferry Ossendorp [b, *], Wim E. Hennink [a, *]

[a] Department of Pharmaceutics, Utrecht Institute for Pharmaceutical Sciences, Utrecht University, Utrecht, The Netherlands
[b] Department of Immunohematology and Blood Transfusion, Leiden University Medical Center, Leiden, The Netherlands
[c] Department of Radiology, Leiden University Medical Center, Leiden, The Netherlands
[d] Leiden Institute of Chemistry, Leiden University, Leiden, The Netherlands
[e] Division of Drug Delivery Technology, Leiden Academic Centre for Drug Research, Leiden University, The Netherlands

ARTICLE INFO

Article history:
Received 8 July 2014
Accepted 5 October 2014
Available online 28 October 2014

Keywords:
Antigen delivery
In vivo tracking
Nanoparticles
Near-infrared imaging
pLHMGA

ABSTRACT

Particulate antigen delivery systems aimed at the induction of antigen-specific T cells form a promising approach in immunotherapy to replace pharmacokinetically unfavorable soluble antigen formulations. In this study, we developed a delivery system using the model protein antigen ovalbumin (OVA) encapsulated in nanoparticles based on the hydrophilic polyester poly(lactide-co-hydroxymethylglycolic acid) (pLHMGA). Spherical nanoparticles with size 300–400 nm were prepared and characterized and showed a strong ability to deliver antigen to dendritic cells for cross-presentation to antigen-specific T cells *in vitro*. Using near-infrared (NIR) fluorescent dyes covalently linked to both the nanoparticle and the encapsulated OVA antigen, we tracked the fate of this formulation in mice. We observed that the antigen and the nanoparticles are efficiently co-transported from the injection site to the draining lymph nodes, in a more gradual and durable manner than soluble OVA protein. OVA-loaded pLHMGA nanoparticles efficiently induced antigen cross-presentation to OVA-specific CD8+ T cells in the lymph nodes, superior to soluble OVA vaccination. Together, these data show the potential of pLHMGA nanoparticles as attractive antigen delivery vehicles.

1. Introduction

Immunotherapy aims at the induction or enhancement of cellular immune responses against the target of interest, and has the advantage of a high efficacy and less side effects based on antigen-specificity [1]. One of the challenging aspects in the development of effective strategies for immunotherapy is to secure efficient antigen presentation by dendritic cells (DCs) in a targeted and sustained manner to subsequently result in activation of antigen-specific T cells [2]. Dendritic cells are professional antigen-presenting cells (APCs) and have a pivotal role in the initiation and orchestration of T cell immune responses [3–6]. Immature DCs constantly engulf and process soluble and particulate antigens, as well as necrotic and apoptotic cells via various mechanisms [7]. Upon maturation, DCs migrate to draining lymph nodes and present the processed protein antigens in the form of linear peptide epitopes to CD4$^+$ and CD8$^+$ T cells through major histocompatibility complex (MHC) class I and class II molecules to initiate a proper immune response against the antigens [6,8,9]. The crucial role of DCs in adaptive immunity makes them an important target for the development of antigen vaccines.

The weak immunogenicity of soluble protein antigens has led to the development of carrier systems that aim for DC targeting and intracellular antigen delivery [2,10–17]. Particulate delivery systems have several advantages such as protection of antigen against enzymatic degradation and enhanced uptake by DCs, the possibility of co-delivery of antigen and adjuvants to DCs, and the possibility of introducing targeting ligands on the surface of the particle as well as prolonged antigen delivery for sustained antigen-presentation

* Corresponding authors.
E-mail addresses: F.A.Ossendorp@lumc.nl (F. Ossendorp), W.E.Hennink@uu.nl (W.E. Hennink).
[1] Authors contributed equally.

http://dx.doi.org/10.1016/j.biomaterials.2014.10.043
0142-9612/

by DCs [2,3,7,15,18–22]. Especially biodegradable polymeric nanoparticles (NPs) have been used extensively as antigen delivery vehicles [3,15,19,23]. In particular, particles based on poly(lactic-co-glycolic acid) (pLGA), a biodegradable polyester, have been widely investigated for diverse pharmaceutical applications including protein and antigen delivery [24–29]. Several studies have shown the efficacy of antigen-loaded pLGA particulate systems in the induction of immune responses both *in vitro* and in animal models [18,30,31]. pLGA particles are far more efficient in generating long-lasting $CD8^+$ T cell immunity than soluble antigen and antigen in incomplete Freund's adjuvant (IFA) [32]. Nevertheless, pLGA systems have several drawbacks as peptide/protein-releasing formulations. Upon degradation, acidification inside the particles results in aggregation and denaturation of the loaded peptide/protein [33]. Moreover, peptide/protein encapsulated in pLGA are prone to chemical modifications such as acylation [34,35]. Altogether these drawbacks lead to incomplete release [36] of the content from the particles and possible undesired immunogenicity and other adverse reactions [37]. To overcome pLGA pitfalls, functionalized polyesters such as poly(lactic-co-glycolic-hydroxymethyl glycolic acid) (pLGHMGA) and poly(lactic-co-hydroxymethyl glycolic acid) (pLHMGA) have been developed. These polymers are more hydrophilic than pLGA and therefore degrade faster, do not show a pH drop inside the degrading particles [38] and cause much lower acylation. Moreover, they show complete and faster release in comparison to pLGA particles [39–41].

The fate of vaccines after administration has been investigated in several *in vivo* imaging studies [42–46]. Fluorescence imaging has received considerable attention during the past few years because of its advantages such as the ease of translation from *in vitro* imaging studies and being non-invasive, fast and cost-effective [47–51]. Several *in vivo* near-infrared (NIR) fluorescent dyes have been developed with excitation/emission maxima between 700 and 900 nm to minimize tissue absorbance and light scattering, resulting in increased depth of penetration, low fluorescence background, and high intensity signals [45]. These dyes can be modified or conjugated to antigens or NPs/polymers [50]. A considerable number of vaccine tracking studies with NIR fluorescent dyes focuses on tracking of DCs rather than the vaccine. Moreover, the fluorescent dye is often encapsulated in the particles which brings the risk of dye leakage from the particles [46,52], or is attached to other contrast agents such as superparamagnetic iron oxide particles [53,54]. The use of NIR fluorescent dyes coupled both to the antigen of interest and to the delivery system may therefore be preferred.

In this study, we evaluate the feasibility of polymeric pLHMGA nanoparticles as a protein antigen delivery system. The particulate antigen showed a superior ability to induce antigen cross-presentation to antigen-specific T cells compared to soluble antigen, both *in vitro* and *in vivo*. Using NIR dyes covalently linked to both the nanoparticle and the model protein antigen, we visualized the delivery system and its content in real-time, showing gradual relocation from the injection site to the draining lymph nodes. This shows the potential of pLHMGA nanoparticles as an efficient antigen delivery system for the induction of antigen-specific cellular immune responses and suggests its experimental application in cancer research.

2. Materials and methods

2.1. Materials

Ovalbumin Low Endo™ (OVA, batch X2N13844) was purchased from Worthington, USA. IRDye680RD and IRDye800CW N-hydroxysuccinimide ester (NHS ester) were purchased from LI-COR Biosciences, USA. Alexa647-labeled ovalbumin was obtained from Molecular probes, the Netherlands. 5-Hexyn-1-ol, polyvinyl alcohol (PVA; Mw 30,000–70,000; 88% hydrolyzed), palladium on carbon (Pd/C; 10% wt. loading dry support), tin(II) 2-ethylhexanoate ($Sn(Oct)_2$), copper(I) acetate, dimethyl sulfoxide (DMSO) and tris[(1-benzyl-1H-1,2,3-triazol-4-yl)methyl]amine (TBTA) were obtained from Sigma–Aldrich, USA. Benzyl alcohol, sodium dihydrogen phosphate (NaH_2PO_4) and disodium hydrogen phosphate (Na_2HPO_4) were obtained from Merck, Germany. D,L-Lactide was from Purac, the Netherlands. N,N-dimethylformamide (DMF), chloroform, dichloromethane (DCM), n-propanol, methanol, tetrahydrofuran (THF) and toluene were from Biosolve, the Netherlands. Sodium azide (NaN_3, 99%), sodium hydroxide (NaOH) and sodium dodecyl sulfate 20% (SDS) were purchased from Fluka, the Netherlands. Micro-BCA protein assay kit was obtained from Thermo Fisher Scientific Inc., (USA). Pyrogen-free water was purchased from Carl Roth, Germany. Phosphate buffered saline (1.8 mM NaH_2PO_4, 8.7 mM Na_2HPO_4, 163.9 mM Na^+, 140.3 mM Cl^-) (PBS) was obtained from B Braun, Germany. Toluene and DMF were dried on 3Å molecular sieves prior to use. Chemicals were used as received without further purification, unless otherwise stated. Azide-functionalized water-soluble near-infrared fluorescent dye 10 (azide-NIR10) (Supplementary Figure S1) was prepared as described elsewhere [55] (Experimental details are provided in supporting information).

2.2. Synthesis of polymers

2.2.1. Synthesis of copolymers of 3S-(benzyloxymethyl)-6S-methyl-1,4-dioxane-2,5-dione with D,L-lactide (pLHMGA)

3S-(benzyloxymethyl)-6S-methyl-1,4-dioxane-2,5-dione (benzyloxymethylmethylglycolide) (BMMG) was synthesized as described before [56]. A copolymer of D,L-lactide and BMMG (50:50 M ratio) was synthesized via ring opening polymeriziton at 130 °C using benzyl alcohol as initiator with a 100/1 monomer-to-initiator molar ratio and $Sn(Oct)_2$ as catalyst (Fig. 1) [39,56]. In a typical procedure, vacuum dried monomers (BMMG (2840 mg, 11.35 mmol) and D,L-lactide (1630 mg, 11.35 mmol)) were introduced into a dry schlenk tube under a nitrogen atmosphere. Next, benzyl alcohol (24.5 mg, 0.226 mmol; 223.1 μL from a 109.8 mg/mL stock solution in toluene) and $Sn(Oct)_2$ (45.9 mg, 0.113 mmol; 409.8 μL from a 112 mg/mL stock solution in toluene) were added. Toluene was evaporated under vacuum for 2 h, the tube was closed and immersed into a preheated 130°C oil bath for 16 h while stirring. Next, the obtained polymer was dissolved in 10 mL chloroform and subsequently precipitated in 500 mL cold methanol to remove the unreacted monomers and to precipitate the polymer, which was collected by filtration and vacuum dried to yield 4.5 g (90%) poly(D,L-lactic-co-benzyloxymethylglycolic acid) (pLBMGA). Subsequently, pLBMGA was dissolved in 500 mL THF, and 5 g of 10% w/w Pd/C catalyst was added. The flask was filled with hydrogen in three consecutive steps of

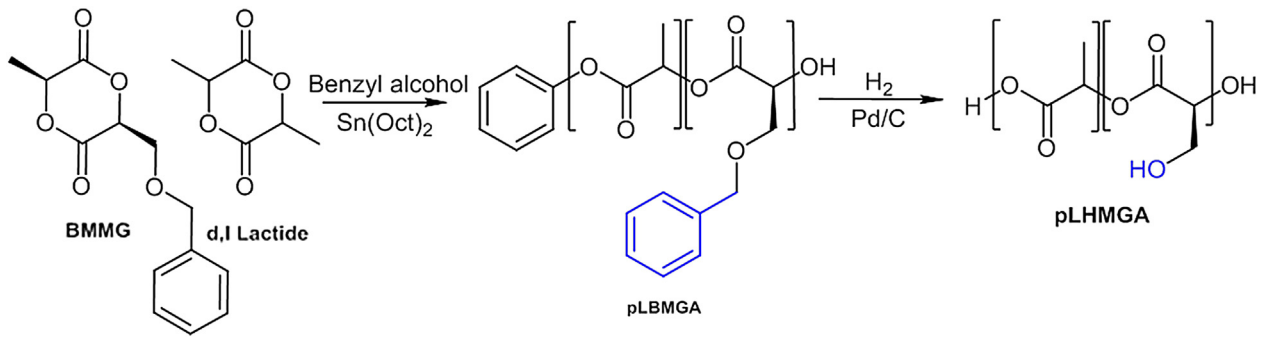

Fig. 1. Synthesis of poly(lactic-co-hydroxymethylglycolic acid) (pLHMGA) in two steps; synthesis of poly(lactic-co-benzyloxymethylglycolic acid) (pLBMGA) via ring opening polymerization of BMMG and D,L-lactide, followed by removing the benzyl group by hydrogenation to yield pLHMGA.

subsequent evacuation and refilling with H_2 and the reaction mixture was stirred for 16 h under a H_2 pressure. Next, Pd/C was removed using a glass filter and THF was removed by evaporation. The obtained polymer was then dissolved in 5 mL chloroform and precipitated in 200 mL n-propanol and vacuum dried after filtration to yield 3 g of pLHMGA (84%).

2.2.2. Synthesis of hexyn-poly(D,L-lactide) (hexyn-pDLLA) to couple to azide-NIR10 via click chemistry

Hexyn-pDLLA was synthesized via ring opening polymerization similar to the method described in section 2.2.1. Briefly, vacuum dried D,L-lactide (396 mg, 2.75 mmol) was transferred into a dry schlenk tube under a nitrogen atmosphere. Next, the initiator, 5-hexyn-1-ol (monomer-to-initiator molar ratio was 70 to 1, 3.85 mg, 0.039 mmol; 75.5 μL from a 51 mg/mL stock solution in toluene) and $Sn(Oct)_2$ (7.9 mg, 0.020 mmol; 71.2 μL from a 112 mg/mL stock solution in toluene) were introduced into the schlenk tube. The tube was evacuated for 2 h, sealed, and immersed in an oil bath thermostated at 130 °C. The polymerization was performed for 16 h and the formed polymer was purified by dissolution in chloroform and precipitation in n-propanol followed by filtration and vacuum drying to yield 370 mg of hexyn-pDLLA (Supplementary Figure S2) (Yield: 92%).

2.3. Conjugation of azide-NIR10 to hexyn-pDLLA by click chemistry

Conjugation of the azide-NIR10 to hexyn-pDLLA was performed using copper catalyzed azide-alkyne cycloaddition [57–60] (Supplementary Figure S3). In a typical procedure, 30.4 mg hexyn-pDLLA (1.84 μmol) and 2 mg azide-NIR10 (1.84 μmol) were transferred into a vial. Then copper (I) acetate (0.2 mol per mole of polymer) and TBTA (0.05 mol per mole of polymer) were added to the vial from their stock solution in dried DMF and the volume was adjusted with DMF to 250 μL. The system was flushed with nitrogen for 20 min and the reaction was performed at 40 °C overnight. The obtained conjugate (NIR10-pDLLA) was purified by precipitation in water. The obtained precipitate was washed with water and freeze-dried at −50 °C and 0.7 mbar overnight (Chris Alpha 1–2 freeze-drier, Germany). The conjugation efficiency was calculated using GPC analysis by dividing the area under the curve of the conjugated polymer using UV detection by the area under the curve of reaction mixture (Yield: 76%).

2.4. Polymer characterization

2.4.1. NMR spectroscopy

A Gemini 300 MHz spectrometer (Varian Associates Inc., USA) was used to conduct ^1H NMR measurements at 298 K. Chemical shifts are reported in ppm with reference to the solvent peak (δ) 7.26 ppm for $CDCl_3$.

2.4.2. Gel permeation chromatography (GPC)

Molecular weight and molecular weight distribution (polydispersity index (PDI); weight average molecular weight/number average molecular weight) of the synthesized pLHMGA was measured by using a Waters Alliance system (Waters, USA) with a Waters 2695 separating module equipped with Waters 2414 refractive index detector. Fifty μL of 5 mg/mL sample was injected onto two PL-gel 5 μm mixed-D columns fitted with a guard column (Polymer Laboratories, M_w range 0.2–400 kDa). Polystyrene standards were used to calibrate the columns and AR grade THF was used as eluent at a flow rate of 1 mL/min and a run time of 30 min. For hexyn-pDLLA and NIR10-pDLLA, DMF containing LiCl 10 mM was used as eluent and a Waters 2478 UV detector was connected to the system and the UV absorbance of the dye was measured at 700 nm. Polyethylene glycol (PEG) standards were used to calibrate the column. The flow rate was set at 0.7 mL/min with a run time of 40 min. The results were analyzed using Empower software v. 2 (Waters, USA).

2.4.3. Differential scanning calorimetry (DSC)

The thermal properties of the polymers were established by using differential scanning calorimetry (Discovery DSC, TA instrument, USA). Two to five mg of polymer sample was loaded into an aluminum pan which was subsequently heated from room temperature to 120 °C, with a heating rate of 5 °C/min, followed by cooling down to −50 °C. Thereafter, the sample was heated to 120 °C with a temperature modulation of ±1 °C and a ramping rate of 2 °C/min. The glass transition temperature (T_g) was recorded as the midpoint of the heat capacity change in the second heating run.

2.5. Labeling OVA with NIR fluorescent dyes

OVA was labeled with either IRDye680RD (IR680) or IRDye800CW (IR800) by coupling the NHS ester of the dyes to the protein. In a typical procedure, 20 mg of OVA was dissolved in 1 mL PBS (B Braun, Germany) pH 7.4 and the pH was adjusted to 8.5 by adding 0.1 mL of K_2HPO_4 1 M pH 9. The IRDye680RD NHS ester was dissolved in DMSO (4 mg/mL) and 0.25 mL of the stock solution containing 1 mg of the dye was added to the OVA solution at a 2:1 molar ratio. The reaction was carried out at room temperature for 2 h. The unreacted dye was subsequently removed with pyrogen-free water by using Zeba™ spin desalting columns equilibrated with pyrogen-free water in two consecutive steps and IR680-OVA was collected after freeze drying (yield: 85%). IR800CW was conjugated and purified by using the same procedure with a dye/OVA feed molar ratio of 1.7 to 1 (yield: 79%).

2.6. Characterization of labeled OVA

IR680-OVA was characterized by GPC using a Waters UPLC Acquity system equipped with a fluorescence detector. Two channels were used: channel 1 for detection of the protein (excitation at 280 nm and emission at 340 nm) and channel 2 for detection of the IR680 signal (excitation at 672 nm and emission at 694 nm). Seven and a half μL of IR680-OVA (10 μg/mL in PBS) was injected onto a BEH450 SEC 2.5 μm column (Waters, USA). PBS was used as elution buffer and the flow rate was set at 0.25 mL/min.

To calculate the dye/OVA molar ratio, the UV spectrum of the freeze-dried labeled OVA was recorded (Shimadzu 2450, Japan) and the absorbance values at 280 nm (A_{280}) and 672 nm (A_{672}) were used to calculate the degree of conjugation according to the following formula:

$$\frac{\text{Dye}}{\text{OVA}} = \left[\!\left[\frac{A_{672}}{\varepsilon_{\text{Dye}}}\right]\!\right] \div \left[\!\left[\frac{A_{280} - 0.07 \times A_{672}}{\varepsilon_{\text{OVA}}}\right]\!\right]$$

Dye/OVA is the molar ratio of IR680 to OVA and the molar extinction coefficient of IR680 (ε_{Dye}) is 165,000 M^{-1} cm^{-1} (according to the manufacturer) and the molar extinction coefficient of OVA (ε_{OVA}) is 30590 M^{-1} cm^{-1} [61].

IR800-OVA was characterized similarly by using the corresponding wavelengths suitable for IR800.

2.7. Preparation of nanoparticles

OVA-loaded nanoparticles (NPs) were prepared by using a double emulsion-solvent evaporation method essentially as described before [62]. In brief, 50 μL of 30 mg/mL OVA solution in pyrogen-free water was emulsified by sonication (30 s, 20 W-ultrasonic homogenizer (Labsonic P, B. Braun Biotech, Germany)) in a solution of 50 mg of pLHMGA in 1 mL of DCM to obtain a water-in-oil emulsion (W_1/O). Next, 2 mL of PVA 1% w/v solution in pyrogen-free water (filtered through a 0.2 μm filter) was added to this first emulsion and a water-in-oil-in-water emulsion was formed by a second round of sonication for 30 s. The double emulsion ($W_1/O/W_2$) was then added dropwise to 25 mL of PVA 0.3% w/v in pyrogen-free water at 40 °C while stirring for rapid removal of DCM. After 1 h, the particles were collected by centrifugation for 30 min at 20,000 g, washed with PBS and consecutively with water, resuspended in pyrogen-free water, and freeze-dried overnight. Dual labeled NPs containing NIR10-labeled pLHMGA and IR680-OVA were prepared using the same method by addition of 4 mg of NIR10-pDLLA to 50 mg of pLHMGA and using IR680-OVA (20 mg/mL) as internal water phase. For preparation of empty NPs or NPs loaded with Alexa 647-OVA, 50 μL pyrogen-free or 50 μL of Alexa 647-OVA was used as internal water phase.

2.8. Nanoparticle characterization

2.8.1. Size and morphology analysis

2.8.1.1. Dynamic light scattering. The size of NPs was measured with dynamic light scattering (DLS) on an ALV CGS-3 system (Malvern Instruments, Malvern, UK) equipped with a JDS Uniphase 22 mW He–Ne laser operating at 632.8 nm, an optical fiber-based detector, and a digital LV/LSE-5003 correlator. Freeze-dried NPs were suspended in deionized water (RI = 1.332 and viscosity 0.8898 cP) and measurements were done at 25 °C at an angle of 90°.

2.8.1.2. Transmission electron microscopy (TEM). The size and morphology of NPs were analyzed by using transmission electron microscopy (TEM, Philips-FEI Tecnai T10, USA). A droplet of nanoparticle suspension in water was placed on a carbon coated copper grid and the sample was stained with 2% uranyl acetate. NPs were visualized with 7–73 k fold magnification and analyzed by MeasureIT software.

2.8.2. OVA content and loading efficiency of NPs

OVA loading efficiency of the NPs was determined by measuring the protein content of digested NPs essentially as described before [63]. In short, about 5 mg of particles (accurately weighed) was dissolved in 0.5 mL of DMSO followed by addition of 2.5 mL of 50 mM NaOH containing 0.5% (w/v) SDS. After complete degradation of the particles, the resulting solution was analyzed by using the Micro-BCA Protein Assay Kit, a calorimetric method that quantifies protein concentration based on peptide bonds and specific amino acid residues. Calibration was done by using 2–40 μg/mL of OVA solution in DMSO:NaOH 50 mM/SDS 0.5% (1:5). Loading efficiency (LE%) is defined as the amount of OVA encapsulated in the nanoparticles divided by the amount of protein added × 100%. Loading percentage (L%) is reported as the amount of OVA entrapped in the particles per total dry mass of the nanoparticles × 100%. In case of dual labeled NPs (containing IR680-OVA) the solution containing the degraded particles was analyzed for its OVA content based on the NIR label by using an Odyssey™ scanner (LI-COR Biosciences, USA) at the 700 nm channel for IR680-OVA and the calibration was done by using IR680-OVA.

2.8.3. In vitro release of OVA from NPs

About 5 mg of freeze-dried dual labeled NPs (containing IR680-OVA) was accurately weighed and suspended in 5 mL phosphate buffered saline (pH 7.4, 49 mM NaH_2PO_4, 99 mM Na_2HPO_4, 6 mM NaCl and 0.05% (w/v)). The particle suspension was incubated at 37 °C under mild agitation. At different time points, 300 μL was removed and centrifuged at 24,000 g for 15 min. The amount of protein released and present in the supernatant was quantified by using an Odyssey™ scanner using the 700 nm channel for visualization of IR680-OVA. Calibration was done by using IR680-OVA in PBS.

2.9. Mice and cells

WT C57BL/6 (CD45.2/Thy1.2; H2-K^b) mice were obtained from Charles River Laboratories (France). Albino BL/6 mice (B6(Cg)-Tyr^{c-2J}/J tyrosinase-deficient immunocompetent BL/6 mice) were bred in the animal breeding facility of the Leiden University Medical Center, the Netherlands. All experiments were approved by the animal experimental committee of Leiden University, the Netherlands. D1 cells are a dendritic cell line of BL/6 background [64], and B3Z is a $CD8^+$ T cell hybridoma specific for the SIINFEKL epitope from OVA and carrying the *lacZ* (*Escherichia coli* β-galactosidase) reporter gene induced by NFAT (nuclear factor of activated T cells) [65]. Antigen-specific activation of B3Z cells leads to T cell receptor-mediated triggering of NFAT, and the subsequent production of β-galactosidase can be quantified by addition of CPRG, a substrate for the β-galactosidase, as a measure of antigen cross-presentation [66]. Cells were cultured in Iscove's Modified Dulbecco's Medium (IMDM, Lonza) containing 8% fetal calf serum (FCS, Greiner), supplemented with 2 mM GlutaMax (Gibco) and 80 IU/mL sodium-penicillin G (Astellas, the Netherlands) for D1 cells, or supplemented with 100 IU/mL penicillin/streptomycin (Gibco), 2 mM glutamin (Gibco), 25 μM 2-mercaptoethanol and 500 μg/mL Hygromycin B (AG Scientific) for B3Z cells. OT-I * Thy1.1 mice are TCR-transgenic mice on B6 background whose $CD8^+$ T cells recognize the OVA epitope SIINFEKL presented in H2-K^b, crossed to Thy1.1 mice to obtain a congenic marker for distinction from endogenous $CD8^+$ T cells in transfer experiments. Naïve OT-I $CD8^+$ T cells were obtained by creating single-cell suspensions from spleens and lymph nodes of OT-I * Thy1.1 mice and subsequent purification of $CD8^+$ cells.

2.10. Dendritic cell viability assay

D1 dendritic cells (50,000 cells/well in 96-well plates) were incubated with dispersions of unlabeled and labeled NPs (7.8–1000 μg/mL) overnight at 37 °C, and cell viability was measured by flow cytometry using the DNA-binding fluorescent dye 7-amino-actinomycin-D (7-AAD) to stain the dead cells.

2.11. Analysis of cellular uptake

D1 cells (100,000 cells/well in 96-well plates) were incubated with Alexa 647-OVA nanoparticles (final concentration of OVA in the medium was 6 μg/mL) overnight. D1 cells were subsequently transferred onto a confocal slide without washing or fixation. The intracellular localization of NPs was studied by confocal laser scanning microscopy imaging using inverted Leica SP2 confocal microscope and the samples were analyzed using the corresponding Leica confocal software in DIC mode.

2.12. In vitro antigen cross-presentation assay

In vitro cross-presentation of OVA by DCs was studied by incubating titrated amounts of OVA encapsulated in NPs or in soluble form with 50,000 D1 cells (100 μL of OVA 0.2–25 μg/mL in PBS corresponding to 0.12–1.5 mg/mL of NPs) for two hours at 37 °C followed by addition of 50,000 B3Z cells and incubation overnight at 37°C in 96-well plates. The cells were then incubated with a lysis buffer containing the CPRG substrate for *lacZ* (PBS +1% 9 mg/mL CPRG + 0.9% 1M $MgCl_2$ + 0.125% NP40 + 0.71% 14.3M β-mercaptoethanol) at 37 °C until the color reaction had progressed sufficiently for readout in a plate reader measuring the optical density at 590 nm. The direct MHC-binding minimal epitope SIINFEKL (100 ng/mL in PBS) was used as a positive control, and unstimulated D1 cells were negative controls.

2.13. In vivo tracking of labeled NPs

Albino BL/6 mice were vaccinated subcutaneously with 50 μg OVA encapsulated in dual labeled NPs dispersed in 100 μL PBS or 50 μg/100 μL PBS IR800-OVA. Vaccine kinetics were then studied at several time points after administration by using the IVIS spectrum preclinical *in vivo* imaging system (PerkinElmer). Kinetics were measured by quantifying the fluorescent intensity in pre-set regions of interest (ROI) at the injection site and the two vaccine-draining inguinal lymph nodes, expressed as the total radiant efficiency in [p/s]/[μW/cm^2]. The fluorescent signal in the injection site at each time point is presented as the as percentage of the maximum recorded value, to show percentual decrease in time. In the lymph nodes the data is presented as the signal to background ratio and it is calculated by dividing the fluorescence signal of the lymph nodes by the background signal at each time point [67].

2.14. In vivo antigen cross-presentation

To establish antigen presentation *in vivo*, BL/6 mice were vaccinated with OVA encapsulated in NPs or in its soluble form. Mice were injected subcutaneously with 200 μL of a 2 mg/mL suspension of NPs in PBS containing 50 μg of encapsulated OVA or 50 μg of soluble OVA. One day after vaccination, 500,000 OVA-specific OT-I $CD8^+$ T cells were injected intravenously in the tail vein in 200 μL PBS. Mice were sacrificed 4 days after T cell transfer to analyze the expansion of the transferred OVA-specific T cells caused by presentation of the OVA antigen. Vaccine-draining inguinal lymph nodes and the spleen were taken out, mashed on 70 μm cell strainers (Becton Dickinson) and the cells were stained with fluorescently labeled antibodies for CD8β and the OT-I congenic marker CD90.1 (Thy1.1), and analyzed by flow cytometry. T cell expansion is expressed as the number of transferred (OT-I) T cells as a percentage from total $CD8^+$ T cells [68].

2.15. Statistical analysis

GraphPad Prism software was used for statistical analysis. Two groups were compared by unpaired two-tailed Student's *t*-test with alpha = 0.05. Statistical significance was considered when $p < 0.05$.

3. Results and discussion

3.1. Synthesis and characterization of pLHMGA

A random copolymer of BMMG and D,L-lactide was synthesized by using BnOH and $Sn(Oct)_2$ as initiator and catalyst, respectively, via ring opening polymerization in the melt (Fig. 1) and the polymer was obtained in high yield (~100%). The protective benzyl groups were subsequently removed overnight by hydrogenation to yield pLHMGA (83%). The structures of the synthesized polymers were confirmed by ^{1}H NMR spectroscopy and this analysis showed that the molar ratio of BMMG and D,L-lactide in pLBMGA (protected polymer) was 48/52, which is close to feed ratio (50/50). Both pLBMGA and pLHMGA were amorphous with T_g values of 39 °C and 57 °C, respectively, which were similar to values reported earlier [39] and confirmed the random structure of the polymers. GPC analysis showed that the number average molecular weight of pLHMGA (16.2 kDa) was close to the aimed molecular weight based on monomer-to-initiator molar ratio (15.8 kDa) and the PDI was 1.6 (Supplementary Table S1). Based on previous studies using the same polymers, we selected a polymer with a relatively low molecular weight in order to achieve small nanoparticles with high loading and fast release.

3.2. Synthesis and characterization of hexyn-pDLLA and NIR10-pDLLA

An alkyne-bearing homopolymer of D,L-lactide (hexyn-pDLLA) was synthesized by using 1-hexyn-6-ol as initiator and $Sn(Oct)_2$ as catalyst. The alkyne functionality in this polymer provides the possibility to conjugate azide-bearing molecules via click chemistry. The obtained polymer was amorphous with a T_g of 50 °C, similar to values reported in the literature [69]. GPC analysis showed that the number average molecular weight of hexyn-pDLLA (11.0 kDa) was close to that of the aimed molecular weight based on monomer-to-initiator molar ratio (10.1 kDa) (Supplementary Table S2).

To obtain a NIR fluorescent-labeled polymer, the azide-NIR10 was coupled to hexyn-pDLLA by click reaction. Analysis of the reaction mixture after 16 h by GPC with UV detection confirmed the presence of labeled polymer at a retention time of 20 min corresponding to that of the polymer, while a peak was also observed at 23.5 min, which corresponds to the retention time of the free dye. From the chromatogram a coupling efficiency of 85% was calculated. After purification, GPC analysis showed that the polymer contained 8% of free dye. GPC analysis of the freeze-dried particles containing NIR10-pDLLA showed that only a negligible amount of free dye was present in the particles indicating that most of the free

Table 1
Characteristics of NPs. Representative data are presented as average ± SD ($N = 3$).

NPs	Size (nm) (DLS)	PDI (DLS)	Loading (L) %	LE% (Loading efficiency)
Empty NPs	364 ± 40	0.22 ± 0.08	–	–
OVA NPs	340 ± 4	0.19 ± 0.04	1.71 ± 0.01	57.4 ± 0.4
Dual labeled NPs	293 ± 3	0.15 ± 0.02	1.38 ± 0.01	69.0 ± 0.4
Alexa-OVA NPs	384 ± 20	0.33 ± 0.05	1.15 ± 0.02	57.6 ± 0.4

dye was removed during particle preparation process (Supplementary Figure S4, and supplementary Table S3).

3.3. Characterization of IR680-OVA and IR800-OVA

In order to prepare a traceable OVA for *in vivo* imaging, the NHS ester of IRdye680RD was conjugated to OVA and the obtained IR680-OVA was analyzed by GPC. Overlapping peaks corresponding to OVA (excitation 280 and emission 340 nm) and IR680 (excitation 672 and emission 694 nm) in the GPC chromatogram of the purified IR680-OVA confirmed that the IR680 was indeed conjugated to OVA (Supplementary Figure S5). No additional peaks (fluorescence detection) were observed, indicating that the free dye was completely removed by purification. Conjugation efficiency calculated by UV measurements showed an average molar dye/protein ratio of 1.7. IR800-OVA was successfully prepared and purified as described for IR680-OVA. The average molar dye/protein ratio was 1.0 (Supplementary Table S4).

3.4. Preparation and characterization of empty and OVA-loaded NPs

Empty and OVA-loaded NPs particles were prepared by a double emulsion-solvent evaporation method, which is a well-known procedure and has been used frequently for encapsulation of hydrophilic drugs as well as biotherapeutics [70–73]. Empty and OVA-loaded NPs with NIR fluorescent dyes on the polymer and/or the protein antigen had comparable characteristics in terms of morphology and size. DLS analysis showed that the mean hydrodynamic diameter of the NPs ranged from 290 to 370 nm with a PDI of 0.15–0.33 (Table 1). The particle preparation procedure was optimized in order to obtain nanoparticles with a size of around 300 nm because nanoparticles of this size were most efficient in activation of dendritic cells and inducing a systemic immune response as compared to bigger particles [74]. Analysis of freeze-dried samples with TEM showed spherical NPs with a size ranging from 150 to 250 nm (Fig. 2), which is smaller than the sizes obtained with DLS. This is due to the fact that DLS reports the hydrodynamic diameter of the particles based on scattering intensity which is proportional to the 6th power of the particle diameter, and therefore in polydisperse samples, relatively low scattering

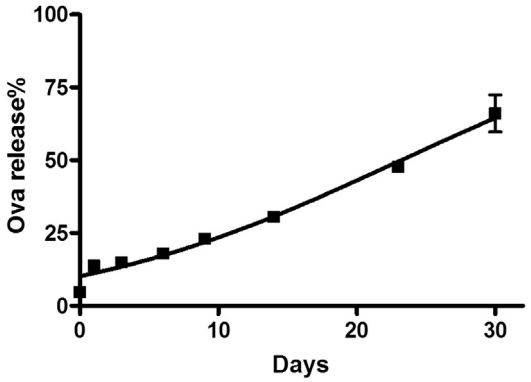

Fig. 3. *In vitro* release of IR680-OVA from pLHMGA NPs. Dual labeled NPs were dispersed in PBS (1 mg/mL) and kept at 37 °C under mild agitation. Following a low burst release of about 5%, IR680-OVA was release in a sustained manner in 30 days up to 70%.

intensities of small particles are overshadowed by high scattering intensities of big particles, resulting in a skewed average size [75,76]. The loading efficiency of unlabeled as well as labeled OVA in NPs was about 60%. The *in vitro* release of OVA from pLHMGA particles was studied by using dual labeled NPs (containing IR680-OVA). Fig. 3 shows that the particles had a low burst release of about 5%, followed by sustained release up to 70% for 30 days. These data are in line with previous studies of pLHMGA particles with the same copolymer composition and loaded with bovine serum albumin [77]. Considering slight variations in the loading efficiency of the nanoparticles and in order to allow a fair comparison in functional experiments, a fixed amount of OVA was used in various *in vitro* and *in vivo* studies.

3.5. Cytocompatibility of empty and OVA-loaded NPs

To assess the cytocompatibility of NPs, dendritic cells were incubated with empty and OVA NPs as well as dual labeled NPs for 16 h at 37 °C. Dead cells were quantified by using 7-AAD, a DNA-binding fluorescent dye which stains cells that have lost membrane integrity [78]. Dendritic cells incubated with LPS and soluble OVA corresponding to the amounts of OVA in the loaded nanoparticles were used as controls. Cell viability was about 90% for dendritic cells incubated with empty and OVA-loaded nanoparticles (concentration of NPs ranging from 7.8 to 1000 μg/mL). These data show the cytocompatibility of these particles.

3.6. Nanoparticle uptake by dendritic cells

To verify that OVA NPs are taken up by dendritic cells, D1 cells were incubated with Alexa647OVA NPs overnight and the

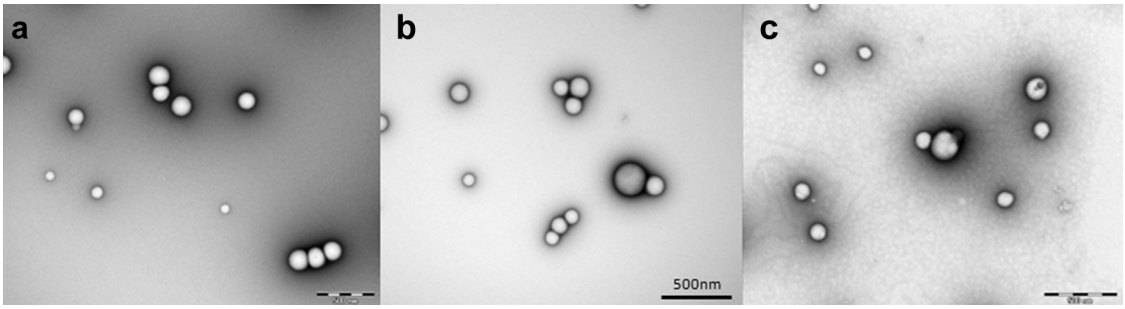

Fig. 2. TEM images of NPs a) Empty NPs, b) unlabeled OVA NPs, c) dual labeled NPs. The bar scale indicates 500 nm.

fluorescent Alexa647 signal was visualized by confocal microscopy. As shown in Figure S6, DCs efficiently take up nanoparticles carrying OVA protein.

3.7. Antigen cross-presentation in vitro

Subsequently, we wanted to test whether the uptake of OVA NPs by DCs leads to processing and cross-presentation of the OVA antigen to OVA-specific T cells. To this end, DCs were incubated with OVA NPs and co-cultured with OVA-specific B3Z hybridoma T cells. Fig. 4 shows that OVA NPs induced antigen-specific T cell activation in a dose-dependent manner, while soluble OVA failed to activate T cells even at high doses. Since this assay is based on the immunological principles of antigen-specificity of T cells, any T cell activation is the result of uptake, processing and cross-presentation of the antigen by DCs to T cells. Furthermore, the dual labeled NPs were equally efficient in T cell activation as the unlabeled NPs (data not shown), showing that labeling did not affect the ability of NPs to induce *in vitro* cross-presentation.

3.8. In vivo tracking of labeled NPs

As our aim was to develop an antigen delivery system that ensures a prolonged supply of antigen to the immune system, we visualized the presence of OVA NPs in the injection site and in the draining lymph nodes, where immune responses are initiated. The tail-base injection site was chosen as it drains specifically to the inguinal lymph nodes which are located at sufficient distance in the mouse to be able to distinguish the injection site from the lymph nodes, and to visualize and quantify their respective signals accurately. Using a dual-color *in vivo* imaging setup based on two distinct NIR fluorescent dyes, we were able to visualize the antigen and the delivery vehicle simultaneously. The NIR fluorescent dye IR680 (excitation 675 nm, emission 720 nm) was coupled to the OVA antigen and the dye NIR10 (excitation 745 nm and emission 840 nm) was coupled to the polymer to track the delivery vehicle. Fig. 5(a) shows the presence of the double-labeled OVA NPs at the injection site in time, compared to a soluble formulation of NIR-labeled OVA protein in PBS. As expected, the vast majority of soluble OVA antigen leaves the injection site within the first day, leading to a short peak presence in the lymph nodes immediately after injection that rapidly decreases (Fig. 5(b)). In contrast, OVA encapsulated in NPs was cleared from the injection site more gradually, corresponding with gradual accumulation in the draining lymph nodes and remaining there for several days. Fig. 6 shows examples of the presence of NP OVA at the injection site and in the draining lymph nodes. Interestingly, the signals from the NP vehicle and its OVA content show similar patterns in the injection site and lymph nodes, suggesting that the OVA antigen arrives in the lymph nodes in encapsulated form. The increasing fluorescent signal of encapsulated IR680-OVA in the first day after injection may be caused by initial quenching of the signal, for example by the hydrophobic environment in the NPs or by self-aggregation and

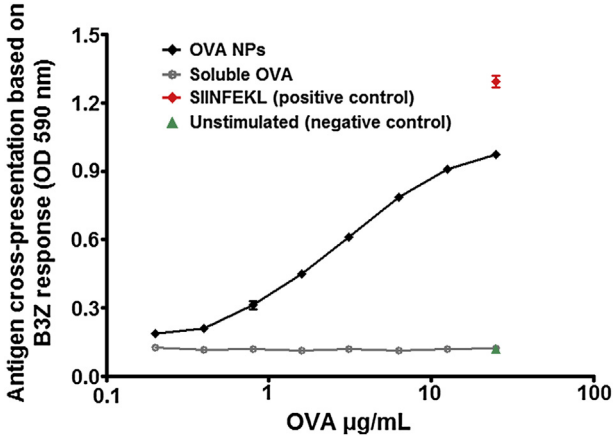

Fig. 4. *In vitro* protein cross-presentation of OVA-encapsulated NPs. DCs were incubated with 0.2–25 µg OVA/mL encapsulated in NPs or in soluble form, and co-cultured with OVA-specific B3Z hybridoma T cells overnight. The B3Z cells contain a construct in which triggering of the T cell receptor, by cross-presentation of their specific OVA-epitope SIINFEKL by DCs, leads to the production of the enzyme β-galactosidase that mediates a color reaction upon addition of the substrate CPRG. This color reaction, measured as the optical density (OD) at 590 nm, therefore forms a measure for antigen cross-presentation by DCs to specific T cells. The SIINFEKL minimal peptide epitope (100 ng/mL in PBS) was used as a positive control, and unstimulated DCs with B3Z cells formed the negative control. $N = 3$ samples per condition, representative graph of 5 independent experiments.

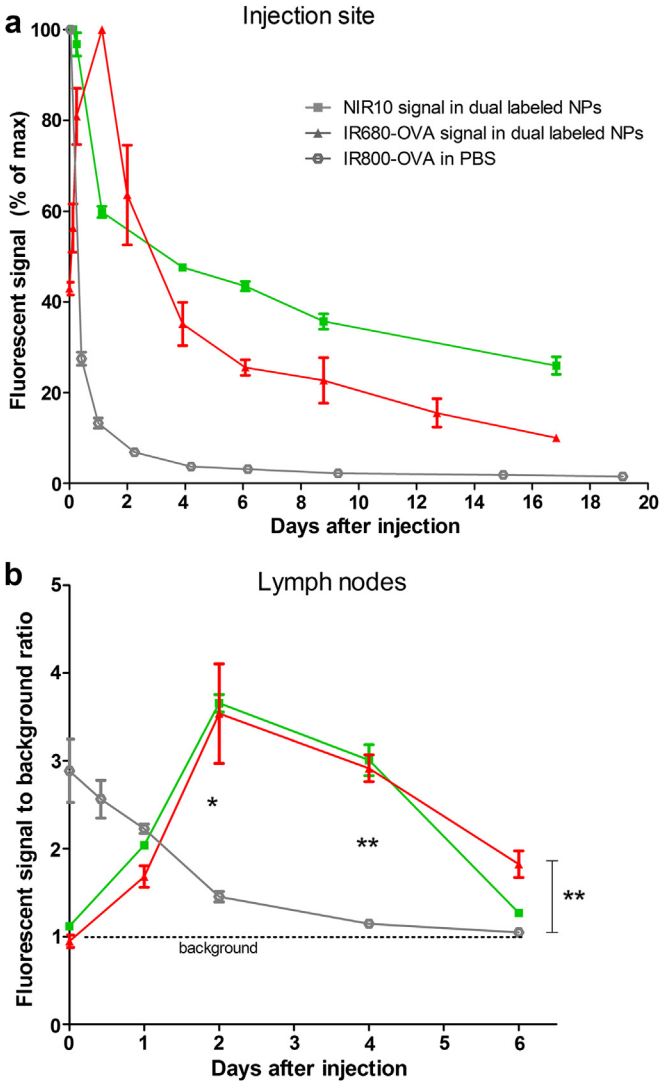

Fig. 5. *In vivo* tracking of NPs and OVA antigen. Quantification of the fluorescent signal of IR680 and NIR10 in dual labeled NPs (containing NIR10 dye on the polymer and IR680 on the OVA), and IR800 signal of soluble antigen (IR800-OVA in PBS) after s.c. injection of 50 µg OVA in NPs or in soluble form. a) Fluorescent signal at the injection site expressed as a percentage of maximum signal. b) Fluorescent signal in the draining lymph nodes expressed as signal to background ratio. Statistical significance is indicated by asterisks comparing IR680 signal in NPs vs soluble IR800-OVA. Statistical analysis was performed by unpaired Student's *t*-test, * = $p < 0.05$, ** = $p < 0.01$. $N = 3$ mice per group.

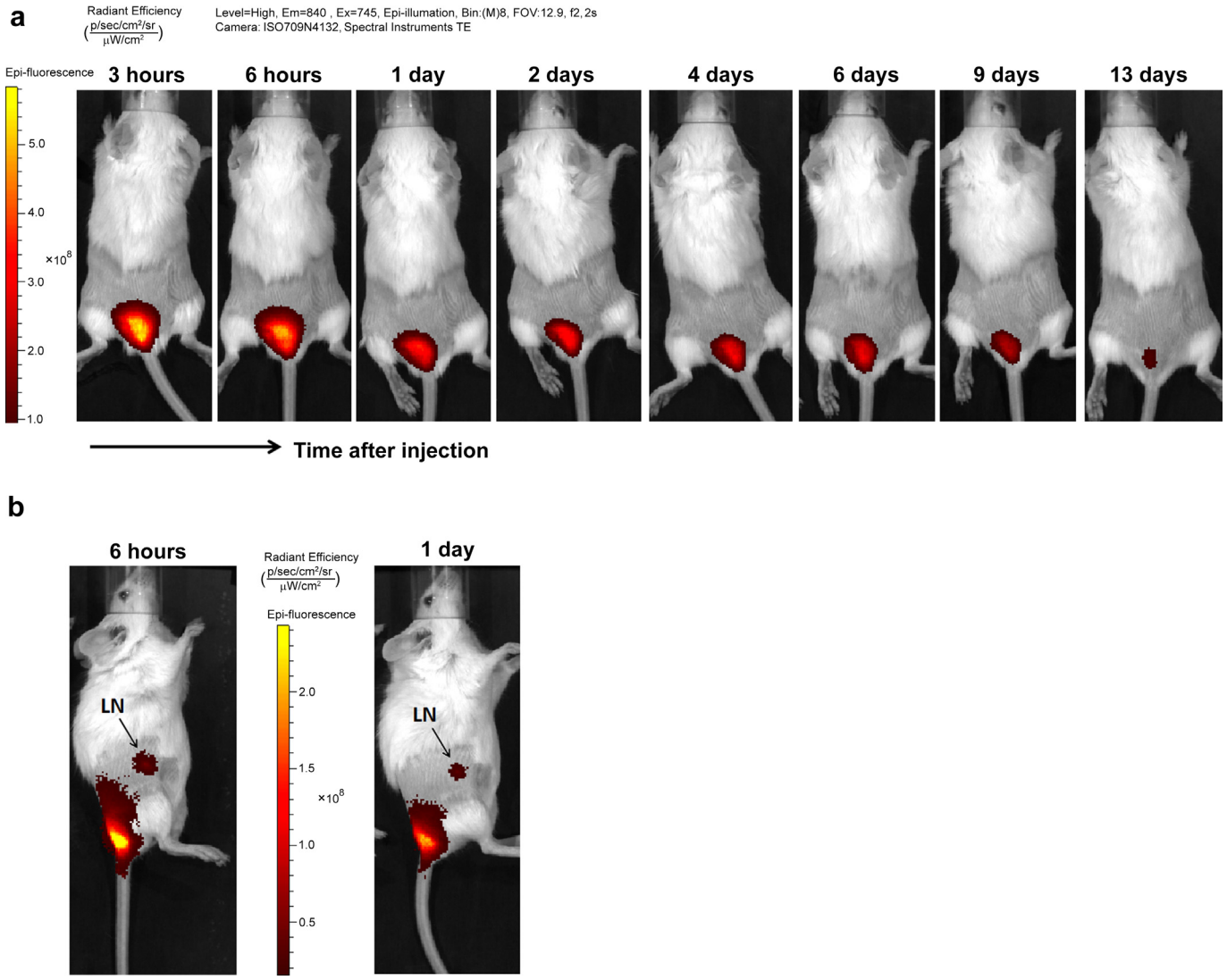

Fig. 6. *In vivo* visualization of OVA NPs in the injection site and draining lymph nodes. Presence of OVA NPs in a) the injection site and b) the right inguinal draining lymph node, based on quantification of the fluorescent signal of NIR10 coupled to the NP polymer. Repeated measurements in time plotted on the same scale of fluorescence. The lymph node (LN) is indicated by an arrow. All images are overlays of grayscale photographs with fluorescence intensity measurements indicated on the color scale. (For interpretation of the references to color in this figure legend, the reader is referred to the web version of this article.)

stacking of the dye at high concentrations [79]. Hydration of the NPs and a decreased stacking of NPs at the injection site during the first day would relieve the IR680 dye from both these quenching effects.

3.9. *In vivo* antigen cross-presentation

The efficient and prolonged delivery of antigen to the draining lymph nodes by OVA NPs led us to test their ability to induce antigen cross-presentation *in vivo*. To test this hypothesis, we administered OVA NPs to mice, followed after one day by an adoptive transfer of OVA-specific CD8+ T cells (OT-I cells). By transferring these high numbers of OT-I T cells, we increase the precursor frequency of OVA-specific T cells to artificially high levels, which allows us to detect subtle effects in terms of cross-presentation of OVA antigen. Four days after T cell transfer, the proliferation of these transferred OT-I T cells as a result of *in vivo* cross-presentation of the OVA antigen was assessed in the vaccine-draining lymph nodes and the spleen (Fig. 7 and Supplementary Figure S7). A strong expansion of OT-I cells was found in the lymph nodes and spleen of mice treated with OVA NPs, which proved far superior to the administration of soluble OVA. The absence of T cell proliferation after injection of equal amounts of empty NPs shows that the delivery system itself plays no role and emphasizes the antigen-specific nature of T cell activation. These results correspond with the superior ability of OVA NPs over soluble OVA to induce *in vitro* antigen cross-presentation to OVA-specific CD8+ T cells (Fig. 4).

4. Conclusion

We developed an antigen delivery system based on pLHMGA nanoparticles encapsulating the model protein antigen OVA. The nanoparticles showed sustained release of antigen *in vitro* and were able to induce *in vitro* antigen cross-presentation by DCs to antigen-specific T cells. Using our non-invasive double-label approach, we visualized the delivery vehicle and the antigen simultaneously in real-time, and showed that the antigen is carried to the lymphoid organs by the delivery vehicle. This finding is in line with the results of *in vivo* antigenpresentation in the lymph nodes, where the OVA

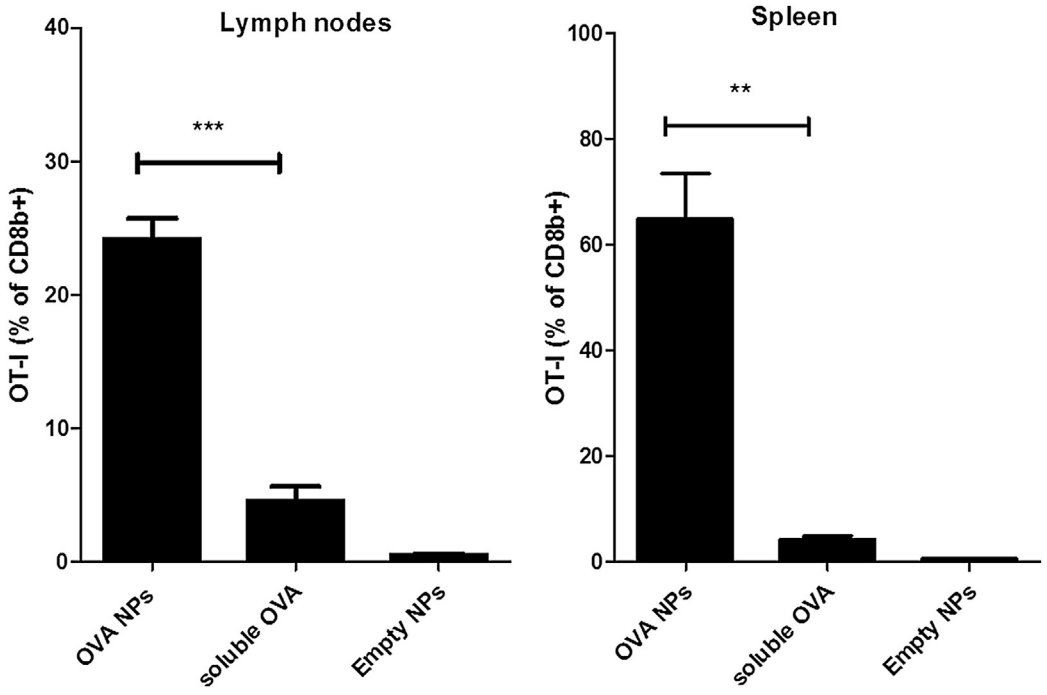

Fig. 7. *In vivo* cross-presentation of OVA antigen to OVA-specific CD8+ T cells. Expansion of TCR-transgenic OVA-specific $CD8^+$ T cells (OT-I) in the draining lymph nodes and spleen, 4 days after transfer into recipients mice. One day before the OT-I transfer, mice were treated subcutaneously with 50 μg OVA either in soluble form or in 400 μg of NPs or with 400 μg of empty NPs. In vivo expansion of the transferred OT-I T cells was quantified by *ex vivo* flow cytometry and expressed as the percentage of the total $CD8^+$ T cell pool (CD8β staining). $N = 3–4$ mice per group, representative of 2 independent experiments. Unpaired Student's *t*-test showed significant difference in OT-I T cell expansion between mice treated with OVA NPs versus soluble OVA, $^{**} = p < 0.01$, $^{***} = p < 0.001$. $N = 3–4$ mice per group.

NPs exhibited a strong capacity to induce antigen-specific $CD8^+$ T cell proliferation through cross-presentation of the antigen. In conclusion, pLHMGA nanoparticles are attractive vehicles for protein antigen delivery for effective stimulation of the cellular immune system.

Acknowledgments

We thank Ana Luisa Silva, Paul Werkhoven, Nataschja Ho and Joep van den Dikkenberg for technical assistance and useful suggestions.

This research was performed within the framework of the Cancer Vaccine Tracking project (#03O-302), Center for Translational Molecular Medicine (CTMM).

Appendix A. Supplementary data

Supplementary data related to this article can be found at http://dx.doi.org/10.1016/j.biomaterials.2014.10.043.

References

[1] Silva JM, Videira M, Gaspar R, Preat V, Florindo HF. Immune system targeting by biodegradable nanoparticles for cancer vaccines. J Control Release 2013;168:179–99.
[2] Reddy ST, Swartz MA, Hubbell JA. Targeting dendritic cells with biomaterials: developing the next generation of vaccines. Trends Immunol 2006;27:573–9.
[3] Akagi T, Baba M, Akashi M. Biodegradable nanoparticles as vaccine adjuvants and delivery systems: regulation of immune responses by nanoparticle-based vaccine. Polym Nanomedicine 2012;247:31–64.
[4] Banchereau J, Briere F, Caux C, Davoust J, Lebecque S, Liu YJ, et al. Immunobiology of dendritic cells. Annu Rev Immunol 2000;18:767–811.
[5] Banchereau J, Palucka A. Dendritic cells as therapeutic vaccines against cancer. Nat Rev Immunol 2005;5:296–306.
[6] Banchereau J, Steinman RM. Dendritic cells and the control of immunity. Nature 1998;392:245–52.
[7] Lanzavecchia A. Mechanisms of antigen uptake for presentation. Curr Opin Immunol 1996;8:348–54.
[8] Vyas JM, Van der Veen AG, Ploegh HL. The known unknowns of antigen processing and presentation. Nat Rev Immunol 2008;8:607–18.
[9] Schuurhuis D, Laban S, Toes R, Ricciardi-Castagnoli P, Kleijmeer M, van der Voort E, et al. Immature dendritic cells acquire CD8(+) cytotoxic T lymphocyte priming capacity upon activation by T helper cell-independent or -dependent stimuli. J Exp Med 2000;192:145–50.
[10] Elamanchili P, Diwan M, Cao M, Samuel J. Characterization of poly(D,L-lactic-co-glycolic acid) based nanoparticulate system for enhanced delivery of antigens to dendritic cells. Vaccine 2004;22:2406–12.
[11] Elamanchili P, Lutsiak CME, Hamdy S, Diwan M, Samuel J. "Pathogen-mimicking" nanoparticles for vaccine delivery to dendritic cells. J Immunother 2007;30:378–95.
[12] Gregory AE, Titball R, Williamson D. Vaccine delivery using nanoparticles. Front Cell Infect Microbiol 2013;3.
[13] Bolhassani A, Safaiyan S, Rafati S. Improvement of different vaccine delivery systems for cancer therapy. Mol Cancer 2011;10(3).
[14] Joshi MD, Unger WJ, Storm G, van Kooyk Y, Mastrobattista E. Targeting tumor antigens to dendritic cells using particulate carriers. J Control Release 2012;161:25–37.
[15] Krishnamachari Y, Geary SM, Lemke CD, Salem AK. Nanoparticle delivery systems in cancer vaccines. Pharm Res 2011;28:215–36.
[16] Mahapatro A, Singh DK. Biodegradable nanoparticles are excellent vehicle for site directed in-vivo delivery of drugs and vaccines. J Nanobiotechnol 2011;9:55.
[17] Park YM, Lee SJ, Kim YS, Lee MH, Cha GS, Jung ID, et al. Nanoparticle-based vaccine delivery for cancer immunotherapy. Immune Netw 2013;13:177–83.
[18] Zhang Z, Tongchusak S, Mizukami Y, Kang YJ, Ioji T, Touma M, et al. Induction of anti-tumor cytotoxic T cell responses through PLGA-nanoparticle mediated antigen delivery. Biomaterials 2011;32:3666–78.
[19] Hamdy S, Haddadi A, Hung RW, Lavasanifar A. Targeting dendritic cells with nano-particulate PLGA cancer vaccine formulations. Adv Drug Deliv Rev 2011;63:943–55.
[20] Demento SL, Cui W, Criscione JM, Stern E, Tulipan J, Kaech SM, et al. Role of sustained antigen release from nanoparticle vaccines in shaping the T cell memory phenotype. Biomaterials 2012;33:4957–64.
[21] Melief CJM. Cancer immunotherapy by dendritic cells. Immunity 2008;29:372–83.
[22] van Montfoort N, Camps MG, Khan S, Filippov DV, Weterings JJ, Griffith JM, et al. Antigen storage compartments in mature dendritic cells facilitate prolonged cytotoxic T lymphocyte cross-priming capacity. Proc Natl Acad Sci U S A 2009;106:6730–5.

[23] Ma W, Chen M, Kaushal S, McElroy M, Zhang Y, Ozkan C, et al. PLGA nanoparticle-mediated delivery of tumor antigenic peptides elicits effective immune responses. Int J Nanomedicine 2012;7:1475–87.
[24] Ye M, Kim S, Park K. Issues in long-term protein delivery using biodegradable microparticles. J Control Release 2010;146:241–60.
[25] Giteau A, Venier-Julienne MC, Aubert-Pouessel A, Benoit JP. How to achieve sustained and complete protein release from PLGA-based microparticles? Int J Pharm 2008;350:14–26.
[26] Sinha V, Trehan A. Biodegradable microspheres for protein delivery. J Control Release 2003;90:261–80.
[27] van de Weert M, Hennink WE, Jiskoot W. Protein instability in poly(lactic-co-glycolic acid) microparticles. Pharm Res 2000;17:1159–67.
[28] Brannon-Peppas L, Blanchette J. Nanoparticle and targeted systems for cancer therapy. Adv Drug Deliv Rev 2004;56:1649–59.
[29] Jain R. The manufacturing techniques of various drug loaded biodegradable poly(lactide-co-glycolide) (PLGA) devices. Biomaterials 2000;21:2475–90.
[30] O'Hagan D, Singh M, Gupta R. Poly(lactide-co-glycolide) microparticles for the development of single-dose controlled-release vaccines. Adv Drug Deliv Rev 1998;32:225–46.
[31] Rosalia RA, Silva AL, Camps M, Allam A, Jiskoot W, van der Burg SH, et al. Efficient ex vivo induction of T cells with potent anti-tumor activity by protein antigen encapsulated in nanoparticles. Cancer Immunol Immunother 2013;62:1161–73.
[32] Mueller M, Schlosser E, Gander B, Groettrup M. Tumor eradication by immunotherapy with biodegradable PLGA microspheres-an alternative to incomplete Freund's adjuvant. Int J Cancer 2011;129:407–16.
[33] Ding AG, Schwendeman SP. Acidic microclimate pH distribution in PLGA microspheres monitored by confocal laser scanning microscopy. Pharm Res 2008;25:2041–52.
[34] Sophocleous AM, Zhang Y, Schwendeman SP. A new class of inhibitors of peptide sorption and acylation in PLGA. J Control Release 2009;137:179–84.
[35] Houchin ML, Topp EM. Chemical degradation of peptides and proteins in PLGA: a review of reactions and mechanisms. J Pharm Sci 2008;97:2395–404.
[36] Kim HK, Park TG. Microencapsulation of human growth hormone within biodegradable polyester microspheres: protein aggregation stability and incomplete release mechanism. Biotechnol Bioeng 1999;65:659–67.
[37] Hermeling S, Crommelin DJA, Schellekens H, Jiskoot W. Structure-immunogenicity relationships of therapeutic proteins. Pharm Res 2004;21:897–903.
[38] Liu Y, Ghassemi AH, Hennink WE, Schwendeman SP. The microclimate pH in poly(D,L-lactide-co-hydroxymethyl glycolide) microspheres during biodegradation. Biomaterials 2012;33:7584–93.
[39] Ghassemi AH, van Steenbergen MJ, Talsma H, van Nostrum CF, Jiskoot W, Crommelin DJA, et al. Preparation and characterization of protein loaded microspheres based on a hydroxylated aliphatic polyester, poly(lactic-co-hydroxymethyl glycolic acid). J Control Release 2009;138:57–63.
[40] Ghassemi AH, van Steenbergen MJ, Barendregt A, Talsma H, Kok RJ, van Nostrum CF, et al. afs controlled release of octreotide and assessment of peptide acylation from poly(D,L-lactide-co-hydroxymethyl glycolide) compared to PLGA microspheres. Pharm Res 2012;29:110–20.
[41] Samadi N, van Nostrum CF, Vermonden T, Amidi M, Hennink WE. Mechanistic studies on the degradation and protein release characteristics of poly(lactic-co-glycolic-co-hydroxymethylglycolic acid) nanospheres. Biomacromolecules 2013;14:1044–53.
[42] Srinivas M, Cruz LJ, Bonetto F, Heerschap A, Figdor CG, de Vries IJM. Customizable, multi-functional fluorocarbon nanoparticles for quantitative in vivo imaging using F-19 MRI and optical imaging. Biomaterials 2010;31:7070–7.
[43] Verdijk P, Scheenen TWJ, Lesterhuis WJ, Gambarota G, Veltien AA, Walczak P, et al. Sensitivity of magnetic resonance imaging of dendritic cells for in vivo tracking of cellular cancer vaccines. Int J Cancer 2007;120:978–84.
[44] Long CM, van Laarhoven HWM, Bulte JWM, Levitsky HI. Magnetovaccination as a novel method to assess and quantify dendritic cell tumor antigen capture and delivery to lymph nodes. Cancer Res 2009;69:3180–7.
[45] Yang Z, Zheng S, Harrison WJ, Harder J, Wen X, Gelovani JG, et al. Long-circulating near-infrared fluorescence core-cross-linked polymeric micelles: synthesis, characterization, and dual nuclear/optical imaging. Biomacromolecules 2007;8:3422–8.
[46] Heo MB, Lim YT. Programmed nanoparticles for combined immunomodulation, antigen presentation and tracking of immunotherapeutic cells. Biomaterials 2014;35:590–600.
[47] Christian NA, Benencia F, Milone MC, Li G, Frail PR, Therien MJ, et al. Vivo dendritic cell tracking using fluorescence lifetime imaging and near-infrared-emissive polymersomes. Mol Imaging Biol 2009;11:167–77.
[48] Frangioni J. In vivo near-infrared fluorescence imaging. Curr Opin Chem Biol 2003;7:626–34.
[49] Escobedo JO, Rusin O, Lim S, Strongin RM. NIR dyes for bioimaging applications. Curr Opin Chem Biol 2010;14:64–70.
[50] Key J, Leary JF. Nanoparticles for multimodal in vivo imaging in nanomedicine. Int J Nanomedicine 2014;9:711–26.
[51] Rao J, Dragulescu-Andrasi A, Yao H, Yao H. Fluorescence imaging in vivo: recent advances. Curr Opin Biotechnol 2007;18:17–25.
[52] Mou Y, Hou Y, Chen B, Hua Z, Zhang Y, Xie H, et al. In vivo migration of dendritic cells labeled with synthetic superparamagnetic iron oxide. Int J Nanomedicine 2011;6:2633–40.
[53] Su H, Mou Y, An Y, Han W, Huang X, Xia G, et al. The migration of synthetic magnetic nanoparticle labeled dendritic cells into lymph nodes with optical imaging. Int J Nanomedicine 2013;8:3737–44.
[54] Chen YC, Wen S, Shang SA, Cui Y, Luo B, Teng GJ. Magnetic resonance and near-infrared imaging using a novel dual-modality nano-probe for dendritic cell tracking in vivo. Cythotherapy 2014;16:699–710.
[55] Lee H, Mason JC, Achilefu S. Heptamethine cyanine dyes with a robust C–C bond at the central position of the chromophore. J Org Chem 2006;71:7862–5.
[56] Leemhuis M, van Nostrum C, Kruijtzer J, Zhong Z, ten Breteler M, Dijkstra P, et al. Functionalized poly(alpha-hydroxy acid)s via ring-opening polymerization: toward hydrophilic polyesters with pendant hydroxyl groups. Macromolecules 2006;39:3500–8.
[57] Kolb H, Finn M, Sharpless K. Click chemistry: diverse chemical function from a few good reactions. Angew Chemie Int Ed 2001;40:2004.
[58] van Dijk M, Rijkers DTS, Liskamp RMJ, van Nostrum CF, Hennink WE. Synthesis and applications of biomedical and pharmaceutical polymers via click chemistry methodologies. Bioconjug Chem 2009;20:2001–16.
[59] Moses JE, Moorhouse AD. The growing applications of click chemistry. Chem Soc Rev 2007;36:1249–62.
[60] Binder WH, Sachsenhofer R. 'Click' chemistry in polymer and material science: an update. Macromol Rapid Commun 2008;29:952–81.
[61] Gill SC, von Hippel PH. Calculation of protein extinction coefficients from amino acid sequence data. Anal Biochem 1989;182:319–26.
[62] Silva AL, Rosalia RA, Sazak A, Carstens MG, Ossendorp F, Oostendorp J, et al. Optimization of encapsulation of a synthetic long peptide in PLGA nanoparticles: low-burst release is crucial for efficient CD8(+) T cell activation. Eur J Pharm Biopharm 2013;83:338–45.
[63] Sah H. A new strategy to determine the actual protein content of poly(lactide-co-glycolide) microspheres. J Pharm Sci 1997;86:1315–8.
[64] Winzler C, Rovere P, Rescigno M, Granucci F, Penna G, Adorini L, et al. Maturation stages of mouse dendritic cells in growth factor-dependent long-term cultures. J Exp Med 1997;185:317–28.
[65] Karttunen J, Sanderson S, Shastri N. Detection of rare antigen-presenting cells by the lacZ T-cell activation assay suggests an expression cloning strategy for T-cell antigens. Proc Natl Acad Sci U S A 1992;89:6020–4.
[66] Shastri N, Gonzalez F. Endogenous generation and presentation of the ovalbumin peptide/k(b) complex to T-cells. J Immunol 1993;150:2724–36.
[67] Filonov GS, Piatkevich KD, Ting L, Zhang J, Kim K, Verkhusha VV. Bright and stable near-infrared fluorescent protein for in vivo imaging. Nat Biotechnol 2011;29:757–61.
[68] Hogquist KA, Jameson SC, Heath WR, Howard JL, Bevan MJ, Carbone FR. T cell receptor antagonist peptides induce positive selection. Cell 1994;76:17–27.
[69] Perego G, Cella GD, Bastioli C. Effect of molecular weight and crystallinity on poly(lactic acid) mechanical properties. J Appl Polym Sci 1996;59:37–43.
[70] Cohen S, Yoshioka T, Lucarelli M, Hwang L, Langer R. Controlled delivery systems for proteins based on poly(lactic glycolic acid) microspheres. Pharm Res 1991;8:713–20.
[71] Mundargi RC, Babu VR, Rangaswamy V, Patel P, Aminabhavi TM. Nano/micro technologies for delivering macromolecular therapeutics using poly(D,L-lactide-co-glycolide) and its derivatives. J Control Release 2008;125:193–209.
[72] Zambaux M, Bonneaux F, Gref R, Maincent P, Dellacherie E, Alonso M, et al. Influence of experimental parameters on the characteristics of poly(lactic acid) nanoparticles prepared by a double emulsion method. J Control Release 1998;50:31–40.
[73] Couvreur P, Puisieux F. Nanoparticles and microparticles for the delivery of polypeptides and proteins. Adv Drug Deliv Rev 1993;10:141–62.
[74] Joshi VB, Geary SM, Salem AK. Biodegradable particles as vaccine delivery systems: size matters. Aaps J 2013;15:85–94.
[75] Dhawan A, Sharma V. Toxicity assessment of nanomaterials: methods and challenges. Anal Bioanal Chem 2010;398:589–605.
[76] Patterson JP, Robin MP, Chassenieux C, Colombani O, O'Reilly RK. The analysis of solution self-assembled polymeric nanomaterials. Chem Soc Rev 2014;43:2412–25.
[77] Ghassemi AH, van Steenbergen MJ, Talsma H, van Nostrum CF, Crommelin DJA, Hennink WE. Hydrophilic polyester microspheres: effect of molecular weight and copolymer composition on release of BSA. Pharm Res 2010;27:2008–17.
[78] Zembruski NCL, Stache V, Haefeli WE, Weiss J. 7-Aminoactinomycin D for apoptosis staining in flow cytometry. Anal Biochem 2012;429:79–81.
[79] Zhegalova NG, He S, Zhou H, Kim DM, Berezin MY. Minimization of self-quenching fluorescence on dyes conjugated to biomolecules with multiple labeling sites via asymmetrically charged NIR fluorophores. Contrast Media Mol Imaging 2014;9:355–62.